# Conduction Studies in Silicon Nitride: Dark Currents and Photocurrents

Abstract: Dark conduction and photoconduction phenomena in amorphous, stoichiometric  $Si_3N_4$  films incorporated into metal-silicon nitride-silicon (MNS) structures are studied in detail. Results demonstrating the importance of hole conduction in  $Si_3N_4$  thin films are presented. The importance of trapped space charge injected from the contacts is shown in an analysis of the effects of  $Si_3N_4$  thickness and the choice of gate metal on conduction. Contact effects that are apparent in the current characteristics of thin  $Si_3N_4$  layers become dominated by bulk conduction mechanisms as the silicon nitride film increases in thickness. Optical interference effects in photoconduction are used to determine the origin of photocarriers.

#### Introduction

Silicon nitride is a wide-bandgap insulator that can be used as a charge storage layer in nonvolatile memories like the metal—silicon nitride—silicon dioxide—silicon (MNOS) structure. In MNOS devices the trapping of electrons or holes in the silicon nitride layer is utilized for information storage. A basic knowledge of the physics of the conduction and trapping properties of this layer is important in understanding the read-write-erase and fatigue characteristics of MNOS devices. In this study, a simple structure with the silicon nitride layer sandwiched between a silicon substrate and a metallic field plate is used to evaluate these properties.

With insulators such as silicon nitride, in which conduction of both electrons and holes and their trapping may be important [1-7], only a broad experimental program using several different techniques can begin to clarify the various physical processes that occur in metal-silicon nitride-silicon (MNS) structures. Photocurrent, dark current, optical interference, and capacitance-voltage techniques are used as part of this investigation of silicon nitride. The first three of these are discussed here and the latter in another publication [8]. In addition, contact electrode material, silicon nitride thickness, and temperature [8] are varied to explore contact and bulk properties of these MNS structures. It is known [9-11] that varying the composition of the Si<sub>3</sub>N<sub>4</sub> films changes their conduction properties. The purpose of this study, however, is to examine in detail only amorphous, stoichiometric films. Preliminary reports of some results from these experiments have been published [1, 2].

The importance of hole injection into and conduction through Si<sub>2</sub>N<sub>4</sub> films is stressed throughout. Early investigators of the conduction properties of Si<sub>2</sub>N<sub>4</sub> films overlooked this and interpreted their results as bulkcontrolled conduction of electrons [9, 12-13]. Recent experiments, however, have shown the important role that holes play in the conduction properties of Si<sub>2</sub>N<sub>4</sub> [1-5, 8]. For negative gate bias, all these experiments indicate a dominant hole conduction mechanism in the Si<sub>2</sub>N<sub>4</sub> film [1-5, 8]. Our internal photoemission experiments under positive gate bias on MNS structures with very thin ( $\approx 200 \text{ Å}$ ) Si<sub>3</sub>N<sub>4</sub> layers [1] and the Weinberg "carrier type" measurements with positive-coronacharged Si<sub>2</sub>N<sub>4</sub> layers on Si substrates with shallow junction detectors [4] both indicated that holes were the dominant charge carrier. On the other hand, Yun's "charge centroid" measurements on MNOS structures with a thin tunnel SiO, layer [3] and the Ginovker et al. carrier type measurements on similar tunnel oxide MNOS structures incorporated into transistor configurations [5] implied that electrons injected from the Si substrate were the dominant charge carrier. These results suggest that for positive gate bias either holes or electrons may be the dominant charge carrier, depending on the experimental situation. This conclusion was also reached in some of our other recent work [2, 8].

In the experimental section of this paper, various results are shown for dark currents and photocurrents in MNS structures with various contact materials and Si<sub>3</sub>N<sub>4</sub> thicknesses. The data indicate a gradual transition from currents that are more contact-limited on the thin-

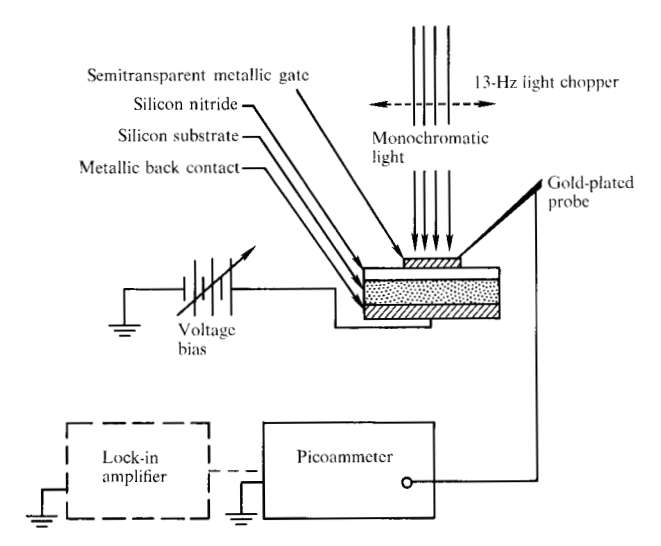


Figure 1 Experimental set-up for photocurrent and dark current measurements. Lock-in amplifier and light chopper were used only for certain experiments.

nest  $\mathrm{Si_3N_4}$  samples ( $\approx 200~\text{Å}$ ) to more bulk-limited on the thickest ( $\approx 3\,000~\text{Å}$ ). Also, extensive photocurrent measurements are described that are performed on MNS structures with thin  $\mathrm{Si_3N_4}$  layers (425 Å) under negative gate bias in a study of the photoexcited hole injection mechanism from the Si substrate into the  $\mathrm{Si_3N_4}$  layer.

In the analysis section, dark current and photocurrent data are modeled for dominant hole injection from the Si under negative gate bias. Also, calculations of optical interference effects in the MNS structures and their relationship to the experimental data and to the origin of photocarriers are described. Reflectances of MNS structures are measured experimentally and compared to theoretical calculations to test the validity of the optical constants (index of refraction and absorption coefficient) used in the analysis in Section 4.

#### 2. Experimental details

 ${\rm Si_3N_4}$  films of thicknesses varying from 220 to 3100 Å, as measured by ellipsometry, were chemically vapor deposited on silicon at 915°C (1188 K) in a hot-wall furnace with a NH $_3$ /SiH $_4$  ratio in the gas phase of 150/1 and a deposition rate of 58 Å/min. Both n and p type (100) silicon substrates were used with resistivities of 0.001 (degenerate) and 2  $\Omega$ -cm with no intentional oxide present, although a native oxide film of less than 15 Å may be present prior to silicon nitride deposition. The gate metallization on the MNS structures was performed at  $10^{-6}$  Torr ( $10^{-4}$  Pa) from an rf-heated crucible to provide circular semitransparent metal dots of Au, Al, or

Mg having an area of  $1.27 \times 10^{-2}$  cm<sup>2</sup> and of thickness 100-270 Å. The spreading resistance across the 50-mil dots on the MNS structures was less than  $60~\Omega$ . Back metallization of Al was added to ensure good electrical contact to the silicon. Optical transmittance of these metal electrodes was determined from metal films that were simultaneously deposited on clean quartz disks during electrode metallization using a calibrated Reeder thermopile and chopped-light techniques. The index of refraction of the  $Si_3N_4$  films was 2.01 as measured by ellipsometry at a wavelength of 5461~Å, which corresponds to what is considered to be a stoichiometric composition [11, 14, 15]. The static dielectric constant of the  $Si_3N_4$  was 7.5 as deduced from MNS capacitance.

The experimental set-up for all the dark and photocurrent measurements is shown in Fig. 1. The light source was a 900-W xenon lamp. A 500-mm Bausch and Lomb grating monochromator blazed at 300 mum, with a reciprocal linear dispersion of 3.3 mµm/mm set for a 5mum bandpass, was used between the xenon lamp and the MNS sample. The image of the monochromator exit slit always completely covered the sample electrode area. This monochromator was equipped with a quartz collimating system at the entrance slit and a quartz achromatic focusing system at the exit slit. Cutoff filters were used to remove second- and higher-order light wavelengths. In some experiments where the light intensity was varied, metal screens were used in front of the sample. For dark current and continuous light photocurrent measurements a Keithly 417 fast picoammeter was used in series with the MNS sample, which was biased using stable mercury batteries. For chopped-light photocurrent measurements, a 13-Hz Bulova light chopper was used, the signal from the MNS structure being detected by a PAR 124 (Princeton Applied Research) lock-in amplifier. In all chopped-light measurements, only MNS structures with degenerate Si substrates were used, and so photoconductive and photovoltaic effects in the Si were negligible. In some measurements where high voltage biases were utilized, the Keithly 417 was used because of its low input impedance (less than 1 mV on any range) between the MNS and the PAR 124 lock-in amplifier to prevent any voltage drop across the PAR 124 input. This instrumental configuration also allowed a simultaneous measurement of small photocurrents and large dark currents.

The sample was held in a vertical position by a vacuum chuck, the direct contact to the 50-mil-diameter semi-transparent metal gate being obtained with a 9-mil-diameter gold plated probe. This probe was positioned near the edge of the metal gate at an angle, as shown in Fig. 1, to minimize shadowing effects in the photocurrent measurements. The samples were measured at room temperature in air and were stored in a nitrogen dry box

when not in use. Under these storage conditions, there were no significant changes in time of the Si<sub>3</sub>N<sub>4</sub> properties reported here.

In transmission and reflection measurements, light incident on and reflected from MNS structures was measured using the thermopile and the chopped-light technique. The light was chopped at 13 Hz and the signal from the thermopile applied to a PAR 190 low noise transformer before being detected by a PAR 124 lock-in amplifier.

# 3. Experimental results

Data for a variety of dark current and photocurrent measurements on MNS structures are presented. The experimental techniques used to produce reproducibility for these measurements from sample to sample are discussed. Although other equally satisfactory data-taking procedures were tried and did lead to detailed differences, the general conclusions reported here still obtain. Reflectance measurements are also described, and their relationship to the optical constants of the MNS structures is shown.

#### · Dark currents

Dark current data are generated by increasing the applied field in 1 MV/cm steps on a virgin location and by measuring the current two min after each step increase. This technique was chosen because of the difficulty in achieving a steady state condition, especially at low fields, which is due to trapped space charge effects in the Si<sub>2</sub>N<sub>4</sub> layer. From capacitance-voltage measurements, the initial charge state of the Si<sub>3</sub>N<sub>4</sub> film for the various MNS structures was found to be approximately neutral after correction for surface states and contact potential differences. This result has also been observed by others [16]. Results of these dark current measurements for different gate metals (Al, Au, Mg), substrate doping (n or p degenerate) and Si<sub>3</sub>N<sub>4</sub> thicknesses (220 to 3100 Å) were reported previously [2], where it was observed that MNS structures with thin Si<sub>3</sub>N<sub>4</sub> layers (220 to 230 Å) sensitively reflect the contact material. Dark current as a function of the magnitude of the average field of  $Al - Si_3N_4 - n$ -degenerate Si and  $Au - Si_3N_4 - n$ -degenerate Si MNS structures for the Si<sub>3</sub>N<sub>4</sub> thickness range studied is shown in Figs. 2 and 3 for both voltage polarities. The average field, Eav, using the Si-Si<sub>3</sub>N<sub>4</sub> interface as the origin of coordinates, is defined as

$$E_{\rm av} = -(V_{\rm g} - \phi_{\rm ms} - \psi_{\rm s})/L, \tag{1}$$

where  $V_{\rm g}$  is the voltage applied to the metal gate,  $\phi_{\rm ms}$  is the metal-silicon work function difference in volts [17, 18], L is the Si<sub>3</sub>N<sub>4</sub> thickness, and  $\psi_{\rm s}$  is the Si surface potential [17, 18]. For degenerate Si substrates,  $\psi_{\rm s}$  is negligible for the average fields of interest.

There are several important features of Figs. 2 and 3 that are used in later sections to show the importance of hole injection from the contacts, a transition from mostly contact- to mostly bulk-limited dark conduction with increasing silicon nitride thickness, and the dominance of hole conduction for negative gate bias:

- For the Al-Si<sub>3</sub>N<sub>4</sub>-n-degenerate Si MNS structures, there is a polarity difference in the dark current data of Figs. 2(a) and 2(b), in which negative gate bias gives larger dark currents. The polarity difference decreases with increasing Si<sub>3</sub>N<sub>4</sub> thickness, due to the contact-limited to bulk-limited transition. This effect has also been seen by others [13, 19, 20]. However, for Au-Si<sub>3</sub>N<sub>4</sub>-n-degenerate Si MNS structures [Figs. 3(a) and 3(b)], the dark currents are approximately identical for both polarities for Si<sub>3</sub>N<sub>4</sub> thicknesses of 425 Å or more because hole injections into Si<sub>3</sub>N<sub>4</sub> from Au and Si encounter a similar interface energy barrier of about 2 eV as compared to Al, which is 3 eV [1, 2, 8].
- 2. For negative gate bias there is little or no dependence on gate metal because of dominant hole injection from the Si. However, for positive gate bias, Au metal gate MNS structures have larger dark currents than comparable Al structures because of hole injection and dependence on the gate electrode. This effect decreases with increasing Si<sub>3</sub>N<sub>4</sub> thickness because of the contact-limited to bulk-limited transition.

Dark current data as a function of average field for  $Al-Si_3N_4-p$ -degenerate Si and  $Al-Si_3N_4-n$ -degenerate Si MNS structures were identical within the reproducibility of the measurement for like polarities for  $Si_3N_4$  thicknesses of 425 Å or more. MNS structures with Mg gate electrodes were studied only for  $Si_3N_4$  thicknesses of 220 and 425 Å, the dark current-average field characteristics for the 425 Å structures being approximately identical to comparable Al gate structures for like polarities.

## • Photocurrents

#### General results

Photocurrent data were generated with either continuous or chopped-light irradiation. For the case of continuous photon irradiation, after application of the voltage bias the dark currents were allowed to decay several hours before the photocurrent measurements were performed point by point from low to high photon energies; the photocurrents were measured approximately one min after each step increase of photon energy. This technique was used because, as was the case with the dark current measurement, charge trapping in the Si<sub>3</sub>N<sub>4</sub> layer at low fields did produce slow transient effects. At an

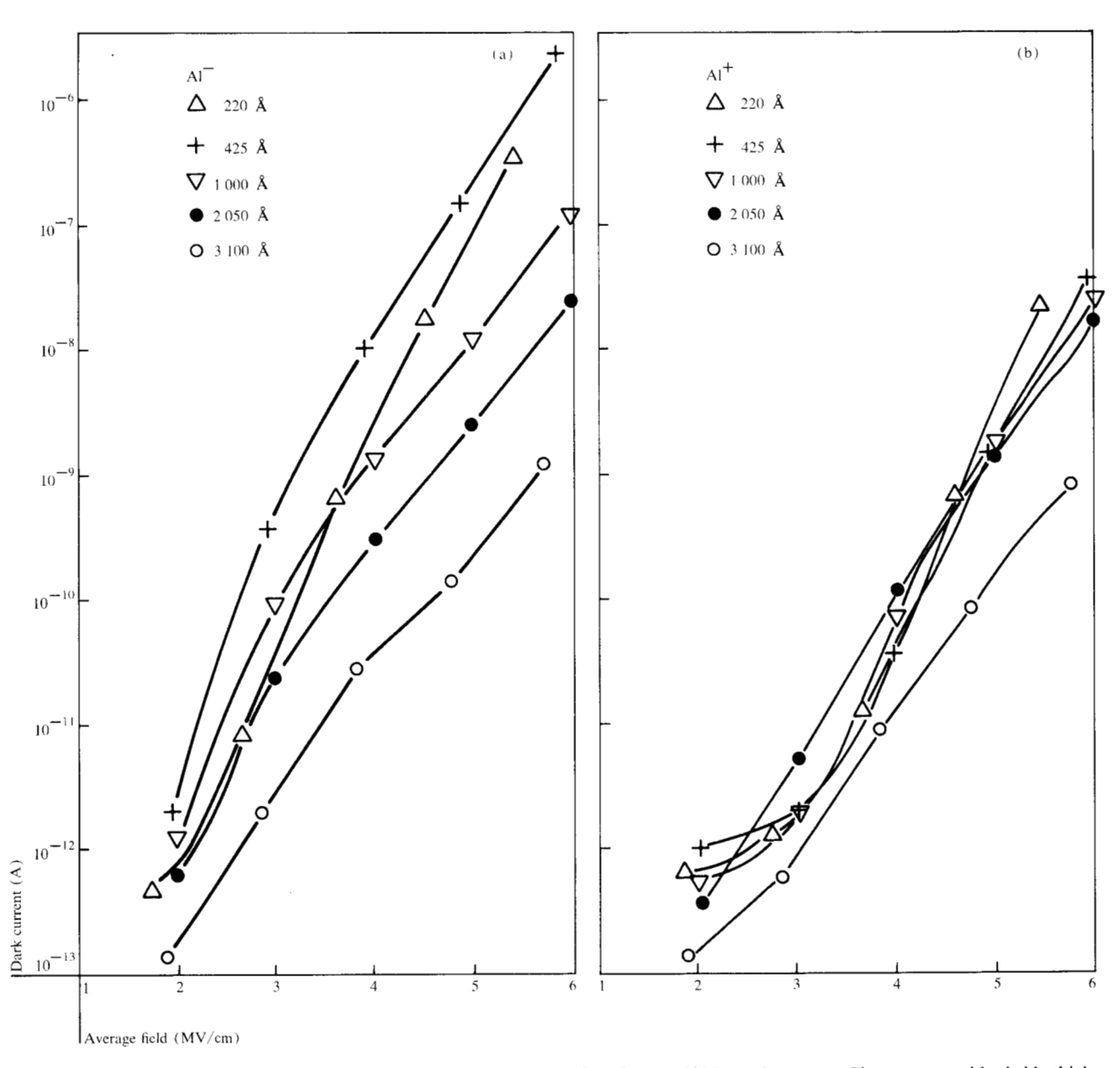


Figure 2 Dark current as a function of the magnitude of the average field for  $Al - Si_3N_4$  – n-degenerate Si structures with nitride thicknesses in the range 220 to 3100 Å. (a) Al negative bias. (b) Al positive bias.

average field magnitude of approximately 3 MV/cm, dark currents became comparable to the largest photocurrents observed and necessitated the use of chopped light techniques at higher fields to resolve photocurrents from large dark currents.

The cube root of the photoresponse as a function of photon energy on thin silicon nitride (220 to 230 Å) MNS structures with various gate metals of Al, Au, Mg and substrate doping (n or p degenerate) was reported previously [1]. The results of these measurements indi-

cated a dominant mechanism of hole internal photoemission, which sensitively reflected the contact material. Cube root photoresponse vs photon energy characteristics on thicker silicon nitride (220 to 3100 Å) MNS structures on 0.001  $\Omega\text{-cm}$  n-Si substrate with both Al and Au gate electrodes for average fields of approximately  $\pm 2$  MV/cm and normally incident light are shown in Figs. 4 and 5. The photoresponse is defined as

$$Y = \frac{I_p \hbar \omega}{S \mathcal{T} A}$$
(photoelectrons/photon), (2)

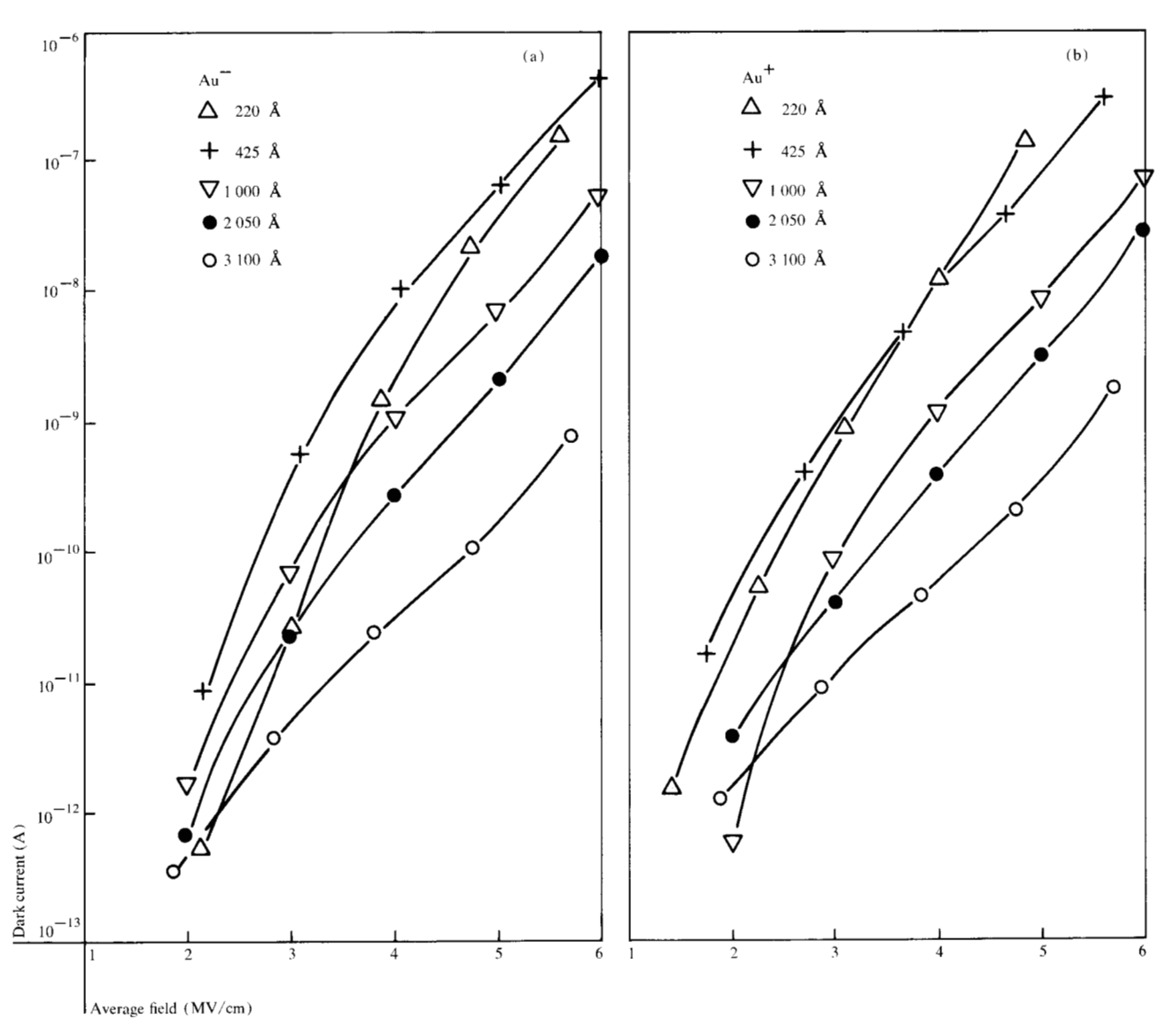


Figure 3 Dark current as a function of the magnitude of the average field for  $Au - Si_3N_4 - n$ -degenerate Si structures with nitride thicknesses in the range 220 to 3100 Å. (a) Au negative bias. (b) Au positive bias.

where  $I_{\rm p}$  is the photocurrent, S is the incident light intensity (power per unit area),  $\mathcal T$  is the transmittance of the semitransparent metal electrode, A is the area of the 50-mil-diameter metal top electrode, and  $\hbar\omega$  is the photon energy. The cube root quantities were used in Figs. 4 and 5 mainly for convenience in comparing and displaying the data. However, this type of plot of the photoresponse also allows one to determine threshold energies under certain assumptions (see section on photocurrents under "Analysis"). There are several important features of Figs. 4 and 5 that are used in later sections to show the importance of hole injection (internal photoemission) from the contacts, a transition from mostly contact (internal photoemission) to mostly bulk-limited (photo-

conductivity) mechanisms with increasing silicon nitride thickness, and the dominance of hole photoconduction for negative gate bias:

1. For MNS structures with silicon nitride thicknesses of 425 Å or greater, for either Al or Au gates, there is a polarity dependence of the photoresponse as a function of photon energy, in which photocurrents for negative gate voltage bias are larger than for positive gate voltage bias. This dependence decreases with increasing silicon nitride thickness, showing a transition from contact-limited to bulk-limited conduction.

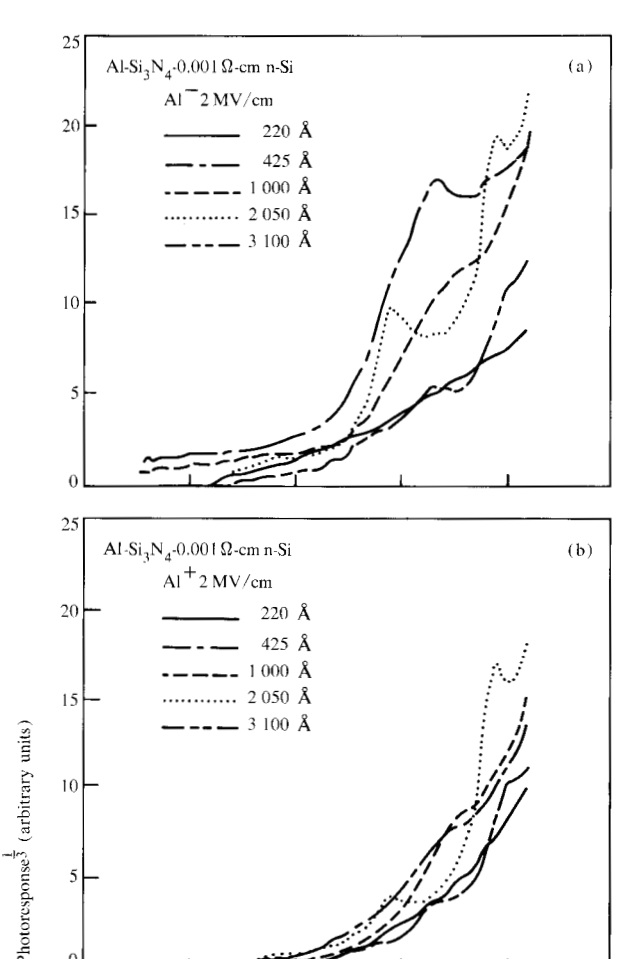


Figure 4 Cube root of the photoresponse as a function of photon energy for Al-Si $_3$ N $_4$ -n-degenerate Si structures with nitride thicknesses in the range 220 to 3100 Å. The magnitude of the average field was 2 MV/cm for all curves. Experimental data were obtained point by point at the same photon energies as shown in Figure 7; lines are used here and in Figure 5 for convenience in comparing samples of varying Si $_3$ N $_4$  thickness. (a) With Al negative bias. (b) With Al positive bias.

Photon energy (eV)

2. The low-energy tail regions of these data for an average field of +2 MV/cm, i.e., negative gate bias, are independent of gate metal (dominant hole injection from the Si). However, data for -2 MV/cm, i.e., positive gate bias, are dependent on gate metal (hole injection from the gate electrode) with photocurrents for Au MNS structures present at lower photon energies. The hole energy barrier for the Au-Si<sub>3</sub>N<sub>4</sub> interface is 1.9 eV as compared to 3 eV for Al-Si<sub>3</sub>N<sub>4</sub> [1, 2, 8]. This dependence decreases with increasing silicon nitride thickness. Again, this is associated

- with the transition from contact-limited to bulk-limited current.
- 3. The structure of peaks and valleys present in the data for photon energies >3.5 eV for silicon nitride thicknesses from 425 to 2910 Å is due to optical interference, which will be verified in the other sections of this paper. The photon energy position of this structure is approximately independent of voltage polarity or gate metal. The currents are due either to photoinjection from the Si or bulk photoconductivity, or both.
- 4. The thickness dependence of the photoresponse for average fields of ±2 MV/cm is very similar to that observed for dark currents on comparable samples. See Figs. 2 and 3.

As was observed on MNS structures with a thin silicon nitride layer of 220 to 230 Å [1], the photoresponse as a function of photon energy for thicker silicon nitride layers is very similar for like polarities (2 MV/cm average field magnitude) for  $Al - Si_3N_4 - n$ - or p-degenerate Si MNS structures. The photoresponse as a function of photon energy for a  $Mg - Si_3N_4 - n$ -degenerate Si structure with a 425 Å nitride layer is very similar to data on a comparable Al gate structure for like voltage polarities at 2 MV/cm average field magnitude. Although thicker silicon nitride samples with Mg gates were not fabricated, this similarity of photocurrents for Mg and Al gate MNS structures for like polarities is expected to hold.

# Results for $425 \text{ Å} - \text{Si}_3 N_4$

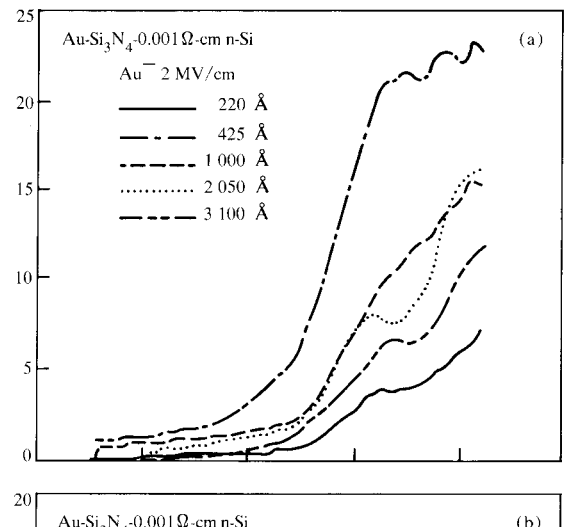
Extensive measurements were made to probe the intensity and voltage dependence of photocurrents for silicon nitride MNS structures 425 Å thick. For negative gate voltage bias, these data are related, in subsequent sections, to a dominant hole internal photoemission mechanism from the Si substrate into the  $\mathrm{Si_3N_4}$  layer. These measurements are discussed in detail in the sections following.

Intensity and high field dependence Photocurrents for an Al-Si<sub>2</sub>N<sub>4</sub>-n-degenerate Si MNS structure with a silicon nitride thickness of 425 Å were linearly dependent on light intensity; the intensity was reduced by up to a factor of 10<sup>2</sup> using metal screens. This linear relationship was observed for average fields of  $\pm 2$ ,  $\pm 3$ , and  $\pm 6$ MV/cm and photon energies of 3, 3.5, 4, and 4.5 eV, and is consistent with internal photoemission [21, 22] as opposed to, for example, space-charge-limited currents, which would be sublinear [23]. Both 13-Hz chopped light (for  $\pm 3$  and  $\pm 6$  MV/cm average fields) and continuous light (for  $\pm 2$  MV/cm average fields) photocurrent techniques were used. Selected data for an average field of 6 MV/cm (negative gate polarity) and photon energies of 3, 3.5, 4, and 4.5 eV are shown in Fig. 6.

The photoresponse as a function of photon energy at  $\pm 6~\text{MV/cm}$  average fields on MNS structures (425 Å of  $\text{Si}_3\text{N}_4$ ) with gate metals of Al, Au, Mg and n- and p-degenerate Si substrates (for p-degenerate Si, only Al- $\text{Si}_3\text{N}_4$ -p-degenerate Si MNS structures) were also obtained. These characteristics at an average field magnitude of 6 MV/cm were similar for like polarities regardless of metal electrode material or substrate doping, as was seen for an average field magnitude of 2 MV/cm. This is discussed in the previous section on general results and shown in Figs. 4 and 5. The strong polarity dependence of the photoresponse-photon energy data for an average field magnitude of 2 MV/cm was also present at 6 MV/cm on these MNS structures for a Si, N<sub>4</sub> layer 425 Å thick.

Photoresponse vs photon energy Photoresponsephoton energy data on MNS structures with thin Si<sub>2</sub>N<sub>4</sub> layers were used to determine the field dependence of hole energy barrier heights at the Si-Si<sub>3</sub>N<sub>4</sub> interface. Figure 7 shows data for an  $Al-Si_3N_4$  (425 Å) - ndegenerate Si MNS structure. The cube root of the photoresponse is given as a function of photon energy for several average fields (Al gate biased negatively) using 13-Hz chopped light. Energy barrier heights,  $q\phi$ , are determined from these data using least squares fits [24] of the linear portions from the low-photon-energy tail region (between 2 and 3 eV) and the intermediate region (between 3 and 4 eV) and are plotted normalized to zero field energy barrier height,  $q\phi_{b0}$  (2.1 or 3.2 eV), as a function of the square root of the field near the injecting contact in Fig. 8. Electron energy barrier heights for a given electric field condition near the injecting interface are determined routinely in this manner for metal-silicon dioxide-silicon (MOS) structures [see Section 4, "Photocurrents" and Eq. (8)]. The insert in Fig. 8 is the zero-field energy band diagram of the MNS structure showing the appropriate energy barriers for hole injection from the Si valence band (2.1 eV) or Si conduction band (3.2 eV) into the Si<sub>2</sub>N<sub>4</sub> valence band. This band diagram was reported previously together with values for metal (Al, Au, Mg) - Si<sub>3</sub>N<sub>4</sub> energy barrier heights for hole injection [1]. The solid curves in Fig. 8 are theoretical calculations of Schottky barrier lowering, including field penetration into the Si [Eq. (9)], and are discussed in Section 4, "Photocurrents." Corrections for optical interference effects in the MNS structure had little effect on the values of the energy barrier heights. These corrections are discussed in detail in later sections.

The appropriate root of the photoresponse used in determining energy barrier heights for internal photoemission is related to the energy distribution of photocarriers at the injecting interface. The method is discussed



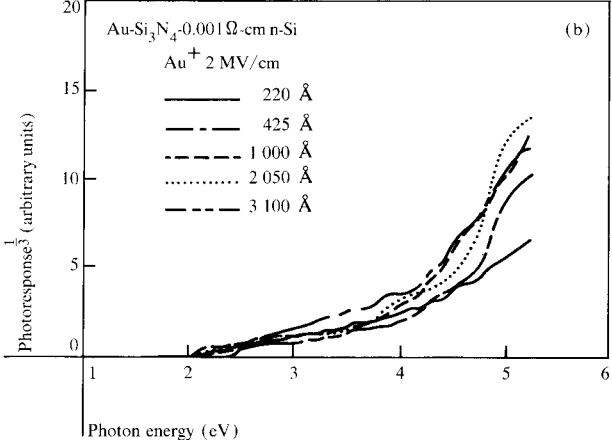


Figure 5 Cube root of the photoresponse as a function of photon energy for  $Au-Si_3N_4$ -n-degenerate Si structures with nitride thicknesses in the range 220 to 3100 Å. The magnitude of the average field was 2 MV/cm for all curves. (a) With Au negative bias. (b) With Au positive bias.

in Section 4, "Photocurrents." This carrier distribution is usually not known exactly. Typically, either cube root or square root plots are used. In comparison to Fig. 8, the energy barrier heights extracted from square root photoresponse-photon energy characteristics were 0.1 to 0.2 eV higher than those extracted from cube root photoresponse-photon energy characteristics having approximately the same standard deviation.

As discussed in Section 4, "Photocurrents," the field near the injecting contact E(0) controls the internal photoemission mechanism under certain assumptions. This field is defined by

$$E(0) = -\left[ \left( V_{\rm g} - V_{\rm fb} - \psi_{\rm s} \right) / L - Q_{\rm ss}^{\,\circ} / \epsilon \right],\tag{3}$$

where E(0) is the field near the contact (which is assumed to be Si for a dominant hole injection mechanism under negative gate voltage bias),  $V_{\rm fb}$  is the flatband

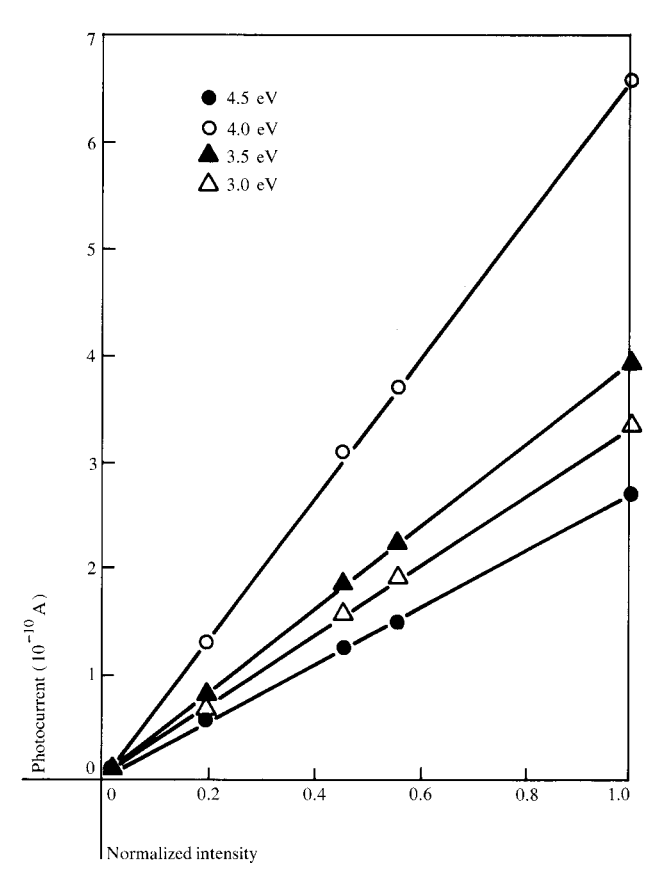


Figure 6 Photocurrent as a function of normalized light intensity for an  $AI-Si_3N_4(425\ \text{Å})-n$ -degenerate Si structure with photon energies from 3 to 4.5 eV at an average field of 6 MV/cm with Al negative bias. The normalization was the value of the light intensity for a given photon energy with no metal screen in place.

voltage,  $Q_{\rm ss}^{\circ}$  is the surface state charge at flat-band, and  $\epsilon$  is the static dielectric constant of the silicon nitride layer. Equation (3), which is discussed elsewhere [8], is derived from the basic equations of MIS capacitors [17, 18]; namely, the voltage drop across the capacitor, the definition of the flat-band voltage, and Poisson's equation at the injecting interface. The last two terms in Eq. (3), i.e., Si surface state charge and surface potential, are small corrections to E(0). When there is no trapped charge in the insulator layer, E(0) is equal to  $E_{\rm av}$  [Eq. (1)].

The internal fields due to trapped space charge, surface state charge, and contact potential differences were determined from measuring flat-band voltages using capacitance-voltage techniques on Al-Si $_3$ N $_4$  (425 Å)-Si MNS structures with both two  $\Omega$ -cm n- and p-Si substrates. These C-V measurements are described in detail in another publication [8]. Flat-band voltages were measured under both dark and various illumination conditions after stressing at the applied voltage bias of interest

for various periods of time. Typical data of the flatband voltage divided by the nitride thickness as a function of the average field for an Al-Si $_3$ N $_4$  (425 Å)-Si (2  $\Omega$ -cm p) structure are shown in Fig. 9. Flat-band voltages in this figure were recorded 1000 s after the application of a negative voltage bias for dark and 2950-Å light conditions. The assumption that internal fields in the 425 Å silicon nitride layer due to trapped space charge would be the same for 2  $\Omega$ -cm and 0.001  $\Omega$ -cm Si MNS structures was verified by comparing dark current and photocurrents which are sensitive to the internal fields [25, 26]. The assumption had been made because C-V measurements are difficult to make with degenerate Si substrates.

Photocurrent vs field In some cases, photocurrentfield data can give information about insulator scattering mechanisms for electrons or holes photoinjected from the contacts. Figure 10 shows photocurrents for photon energies at 3, 3.5, 4, and 4.5 eV as a function of the average field with negative gate voltage bias, in the silicon nitride layer of an Al-Si<sub>3</sub>N<sub>4</sub> (425 Å) - n-degenerate Si MNS structure. These data, obtained with 13-Hz chopped light, were reproducible on a given sample and from sample to sample and did not depend on the order in which the data were taken. Reducing the light intensity by means of screens to varying degrees up to  $10^{-2}$ , changed the data of Fig. 10 only by a scale factor. This is expected and is consistent with the observation previously mentioned of the photocurrents varying linearly with light intensity. Photocurrent data for the same average field range and photon energies as in Fig. 10 were also taken on Al-Si<sub>3</sub>N<sub>4</sub> (425 Å)-p-degenerate Si MNS structures. These data are similar to those of Fig. 10; however, the photon energy dependent saturation and roll-off of photocurrents at high fields were not present. A hole internal photoemission model similar to the electron internal photoemission model of Berglund and Powell [21], which includes hole scattering in the silicon nitride layer, is used in Section 4, "Photocurrents," to arrive at a model consistent with the data of Fig. 10.

Figure 11 shows the logarithm of the photocurrent (from the data of Fig. 10) as a function of  $x_0$ , the position of the potential maximum (zero-field point) in the  $\mathrm{Si}_3\mathrm{N}_4$  as measured from the  $\mathrm{Si}\text{-}\mathrm{Si}_3\mathrm{N}_4$  interface for hole internal photoemission. As discussed in Section 4, "Photocurrents," the zero-field point,  $x_0$ , is approximately inversely dependent on the square root of E(0), the field near the  $\mathrm{Si}$  injecting contact. The linear regions of Fig. 11 for an  $\mathrm{Al}-\mathrm{Si}_3\mathrm{N}_4$  (425 Å) – n-degenerate  $\mathrm{Si}$  structure were fitted by the method of least squares to determine l, the hole scattering length in the  $\mathrm{Si}_3\mathrm{N}_4$ . The insert in Fig. 11 shows the fitted values of l as a function of photon energy. Similarly for  $\mathrm{Al}-\mathrm{Si}_3\mathrm{N}_4$  (425 Å) – p-degenerate  $\mathrm{Si}$ 

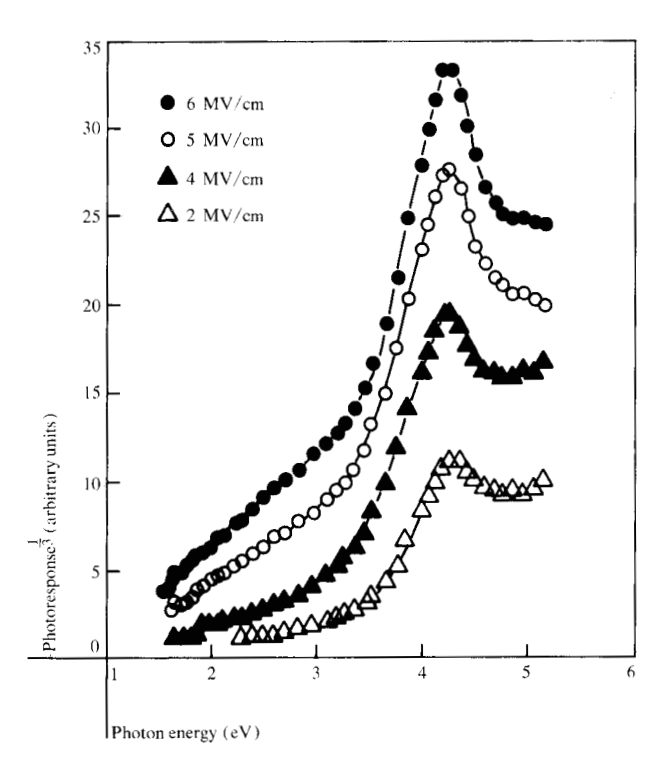


Figure 7 Cube root of the photoresponse as a function of photon energy for the MNS structure of Figure 6 at average fields from 2 to 6 MV/cm with Al negative bias.

structures, fitting the linear region of the logarithm of the photocurrent as a function of  $x_0$  led to values of l within at least 25 percent of those shown in Fig. 11.

# • Reflectance and optical interference

A test was made of the validity of the values for index of refraction and absorption coefficient for Al [27-29], Au [27, 28, 30], Si [31-33], and Si<sub>3</sub>N<sub>4</sub> [34] used in the analysis section for absorptance in the Si or metal layers, reflectance from the MNS structures, and average intensity in the Si<sub>3</sub>N<sub>4</sub> layer. For this purpose the ratios of reflected photon flux to incident flux of the MNS structures in Figs. 4 and 5 were measured for the case of light striking the MNS at a 10° angle of incidence and were compared to those deduced from theoretical calculations. Figure 12 shows selected experimental reflectance data for a Au  $(240 \text{ Å}) - \text{Si}_3\text{N}_4 (2050 \text{ Å}) - \text{n-degenerate}$ Si structure and compares the data to theory, as described in the figure caption. The good agreement between experiment and theory shown in Fig. 12 was found for all the MNS structures of Figs. 4 and 5.

The data of Figs. 4 and 5 were for zero angle of incidence. For other angles of incidence, the peaks in these data, at least for the thicker Si<sub>3</sub>N<sub>4</sub> structures, clearly shifted, as would be expected for optical interference in thin film structures.

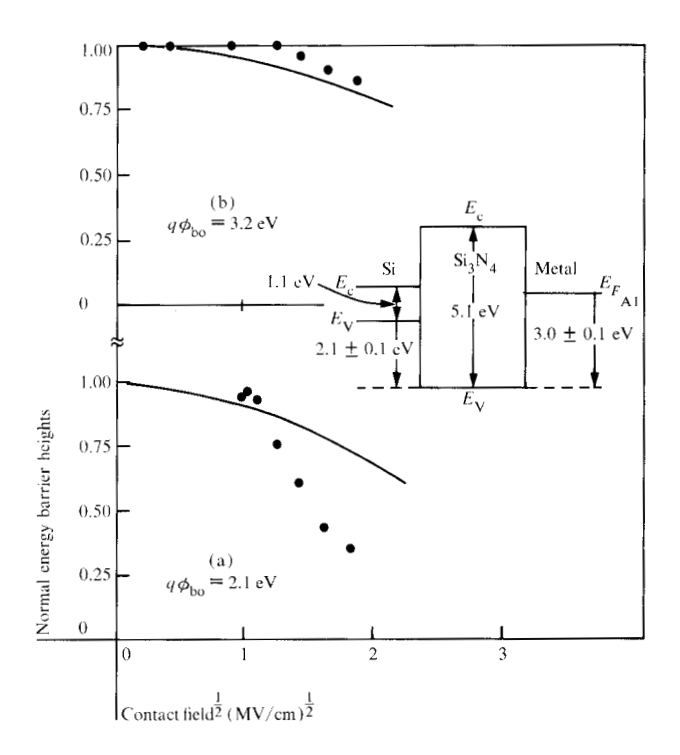
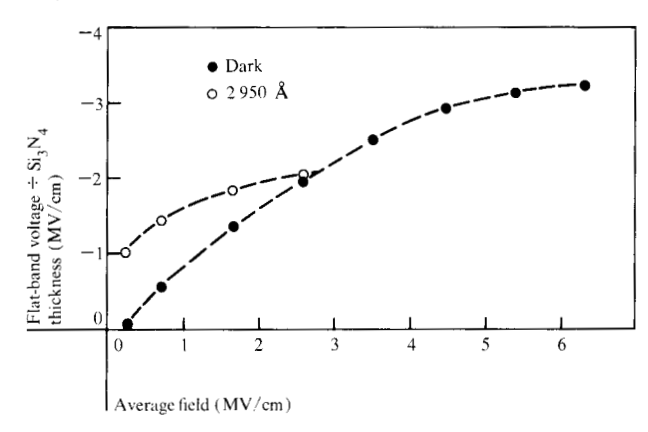


Figure 8 Normalized energy barrier height as a function of the square root of the field near the injecting contact,  $E(0)^{\frac{1}{2}}$ , with Al negative bias for the MNS structure of Figure 6. The normalization was the value of the zero field, energy barrier height,  $q\phi_{b0}$ , namely, 2.1 eV and 3.2 eV for hole internal photoemission from the silicon valence (Figure 8a) and silicon conduction (Figure 8b) bands respectively into the silicon nitride valence band. The solid curves are a theoretical calculation using a simple Schottky barrier lowering model including field penetration into the silicon and are described in the text. The insert is the zero-field energy band diagram taken from Ref. 1.

Figure 9 Flat-band voltage divided by  $Si_3N_4$  thickness as a function of the average field for an Al- $Si_3N_4$ (425 Å) – Si(2 Ω-cm p) structure under dark and 2950 Å light conditions with Al negative bias. Flat-band voltages were recorded 1000 s after application of the voltage bias.



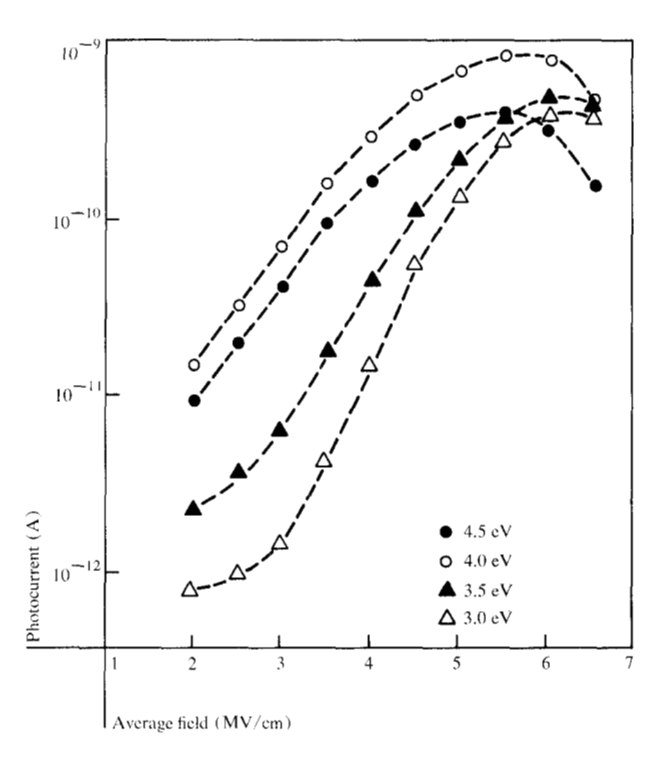
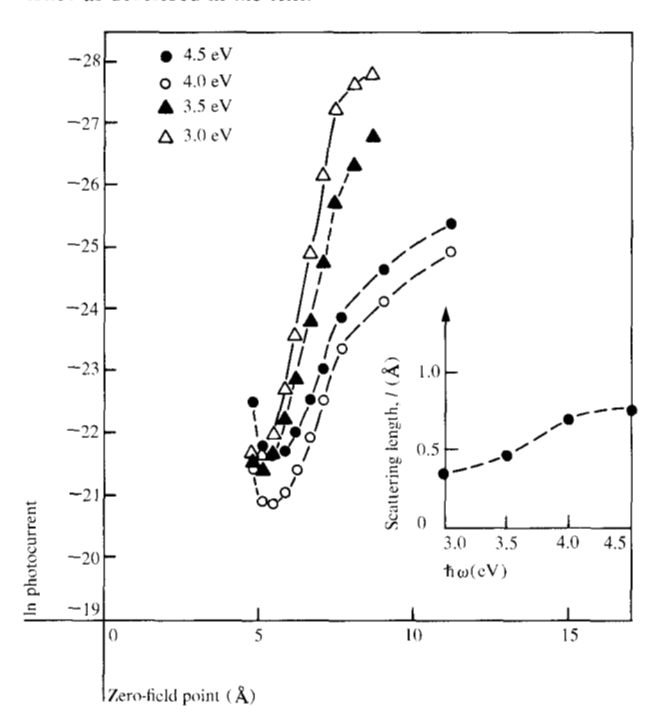


Figure 10 Photocurrent as a function of the average field for the MNS structures of Figure 6 at various photon energies from 3 to 4.5 eV with Al negative bias.

Figure 11 Natural logarithm of the photocurrent in Figure 10 as a function of the zero-field point position with respect to the injecting interface  $(Si-Si_3N_4)$ . The insert shows values of the scattering length, I, as a function of the photon energy from least squares fits of the linear portion of the  $\ln(I_p)-x_0$  characteristics as described in the text.



## 4. Analysis

#### · Dark currents

The analysis of dark currents in MNS capacitors is restricted for simplicity to cases in which one carrier dominates. In silicon nitride injected carriers usually are strongly trapped, giving rise to an insulator space charge that reduces the injection rate. Steady state is reached when the injection rate becomes equal to the rate at which carriers are transported through the insulator by the action of trapping and detrapping. Although the experimental data do not represent a true steady state condition, we will assume the data are sufficiently close to justify assuming the steady state in our analysis.

Under steady state conditions the space charge distribution is constant in time and, therefore, the current is uniform with distance x from the injecting contact into the insulator. It has been shown [35] that space charge due to carriers in the insulator bands at high fields is negligible. Thus, the equations describing steady state reduce to

$$\partial E(x) / \partial x = q n_{t}(x) / \epsilon, \tag{4}$$

$$J \, \hat{\sigma}_{\rm t} \, [N_{\rm t} - n_{\rm t}(x)] = n_{\rm t}(x) \, \nu_0 \, e^{-[\hat{\phi}_{\rm t} - \hat{\beta} \, E(x)^{\frac{1}{2}}]}, \tag{5}$$

where a single trap level is assumed which is  $\phi_t$  below the band edge and has density  $N_t$ . The insulator is assumed neutral with the traps unfilled. Equation (4) is Poisson's equation relating the gradient of the local field E to the trapped charge density  $qn_t$ . Equation (5) equates the trapping rate as given by the product of the current density J, the effective capture cross section  $\hat{\sigma}_t$ , and the number of unfilled traps to the detrapping rate. We assume a Poole-Frenkel (field-assisted thermal ionization) detrapping mechanism, where  $\nu_0$ ,  $\hat{\phi}_t$ , and  $\hat{\beta}$  are the attempt-to-escape frequency, the normalized trap depth  $q\phi_t/kT$ , and the normalized Poole-Frenkel constant  $q[q/\pi\epsilon']^{\frac{1}{2}}/kT$ . q, k, T, and  $\epsilon'$  are the magnitude of electronic charge, Boltzmann's constant, absolute temperature, and the optical dielectric constant, respectively.

The solution of Eqs. (4) and (5) is discussed in detail elsewhere [35], and so we simply restate the results here. Unfortunately, one does not obtain a simple algebraic relation between the current and the average field. Instead, we obtain first a relation between the contact fields and the current

$$(\epsilon/qN_{t}x_{D})[E(L) - E(0)] + \frac{F[E(L)]}{F[E(0)]} e^{\hat{\beta}[E^{\frac{1}{2}}(L) - E^{\frac{1}{2}}(0)]}$$

$$= 1 + L/x_{D},$$
(6)

where

$$x_{\rm D} = [\, \epsilon \nu_{\rm 0} / \, q N_{\rm t} J \hat{\sigma}_{\rm t}] \, \, F[\, E(\, 0)\, ] \, \, e^{-[\hat{\phi}_{\rm t} - \hat{\beta} E^{\frac{1}{2}}(0)]}$$

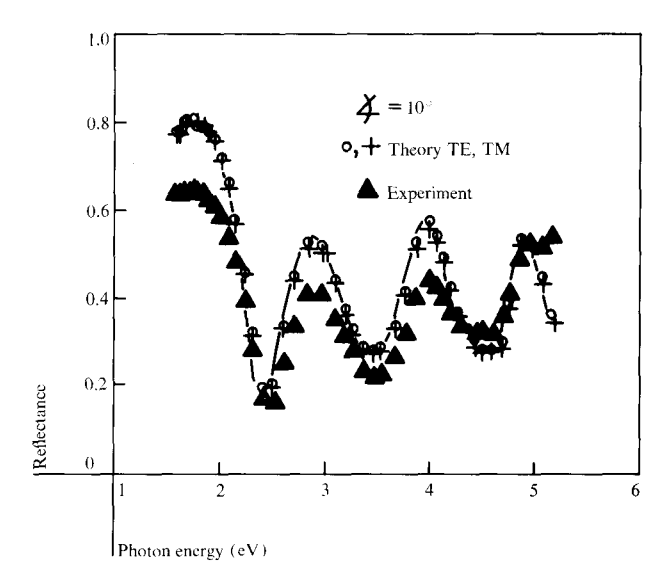


Figure 12 Reflectance at a 10° angle of incidence as a function of photon energy for a Au(240 Å) – Si $_3$ N $_4$ (2050 Å) – ndegenerate Si structure. The solid curve is drawn for clarity in comparing the experimental points (solid triangles) to theoretical calculations (described in the text) for either the transverse electric, TE, wave (open circles) or the transverse magnetic, TM, wave (crosses).

and

$$F[E] = 2[\hat{\beta}E^{\frac{1}{2}} - 1].$$

Second, through the gate voltage, we have a relation between  $E_{\rm av}$ , E(L), E(0), and J

$$\begin{split} E_{\rm av} &= (\epsilon/2qN_{\rm t}L) \ [E(L)^2 - E(0)^2] \\ &+ [\epsilon\nu_0/J\hat{\sigma}_{\rm t}N_{\rm t}L] \ e^{-\hat{\phi}_{\rm t}} \left[F_1[E(L)] \ e^{\hat{\beta}E(L)^{\frac{1}{2}}} \right. \\ &- F_1[E(0)] \ e^{\hat{\beta}E(0)^{\frac{1}{2}}}], \end{split} \tag{7}$$

where

$$F_1[E] = 2[\hat{\beta}^3 E^{\frac{3}{2}} - 3\hat{\beta}^2 E + 6\hat{\beta} E^{\frac{1}{2}} - 6]/\hat{\beta}^4.$$

Equations (6) and (7) can be used to relate  $E_{\rm av}$ , E(0), and J. At this point, one could assume the injecting contact to have a particular J-E(0) dependence, e.g., Fowler-Nordheim, Schottky emission, etc. However, if the injecting contact is at the silicon interface, the J-E(0) relation can be determined by an experiment which measures current and flat-band voltage simultaneously [8]. We have chosen the latter approach and therefore input the experimental J-E(0) relation to calculate J- $E_{\rm av}$  characteristics.

The model contains numerous physical constants, only a few of which can represent independent model parameters. Consequently, we choose reasonable values for  $\nu_0$ ,  $\hat{\sigma}_t$ ,  $\epsilon'$ , and  $\epsilon$  of  $10^{14}/\mathrm{s}$  [36],  $5 \times 10^{-13}$  cm<sup>2</sup> [3, 7], 4  $\epsilon_0$ , and 7.5  $\epsilon_0$ , respectively, and consider  $\phi_t$  and  $N_t$  as

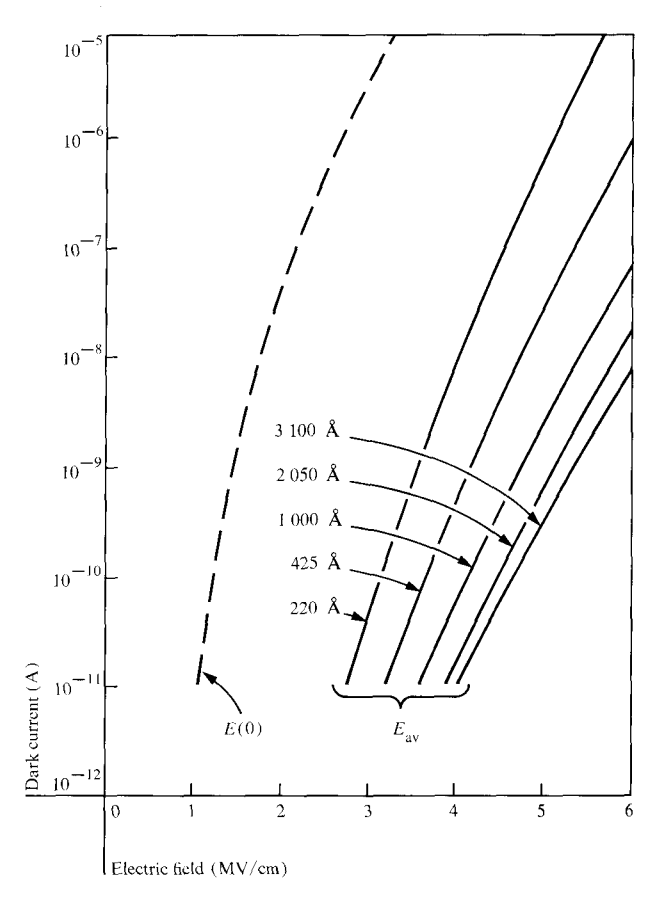


Figure 13 Theoretical calculations of the dark current as a function of the average field,  $E_{\rm av}$ , with nitride thicknesses in the range 220 to 3100 Å and metal gate bias negative. The experimental dark current-contact field, E(0), input data is also shown. The adjustable parameters of trap depth,  $\phi_{\rm t}$ , and trap density,  $N_{\rm t}$ , were 1.63 eV and  $1\times10^{19}~{\rm cm}^{-3}$ , respectively.

adjustable model parameters.  $\epsilon_0$  is the permittivity of free space. Typical results for one choice of parameters are shown in Fig. 13.

The qualitative effect of increasing  $N_{\rm t}$  or  $\phi_{\rm t}$  is to increase the trapped charge density and, consequently, for the same contact field the average field is increased. In detail, the primary effect of increasing  $N_{\rm t}$  is to shift the curves of J vs  $E_{\rm av}$  en masse to higher values of  $E_{\rm av}$ , while increasing  $\phi_{\rm t}$  increases the distance between curves of different thickness. Conversely, as  $\phi_{\rm t}$  or  $N_{\rm t}$  decreases, all curves will collapse toward the J-E(0) characteristic.

The experimental data of Fig. 3(a) should represent the best case for comparison with theory, because for negative Au bias the principal carriers should be holes injected from the silicon. The calculations of Fig. 13 actually represent a best fit to the data of Fig. 3(a), and give parametric values of  $N_{\rm t}=1\times10^{19}~{\rm cm}^{-3}$  and  $\phi_{\rm t}=1.63~{\rm eV}$ . The shallow slope of the experimental curves

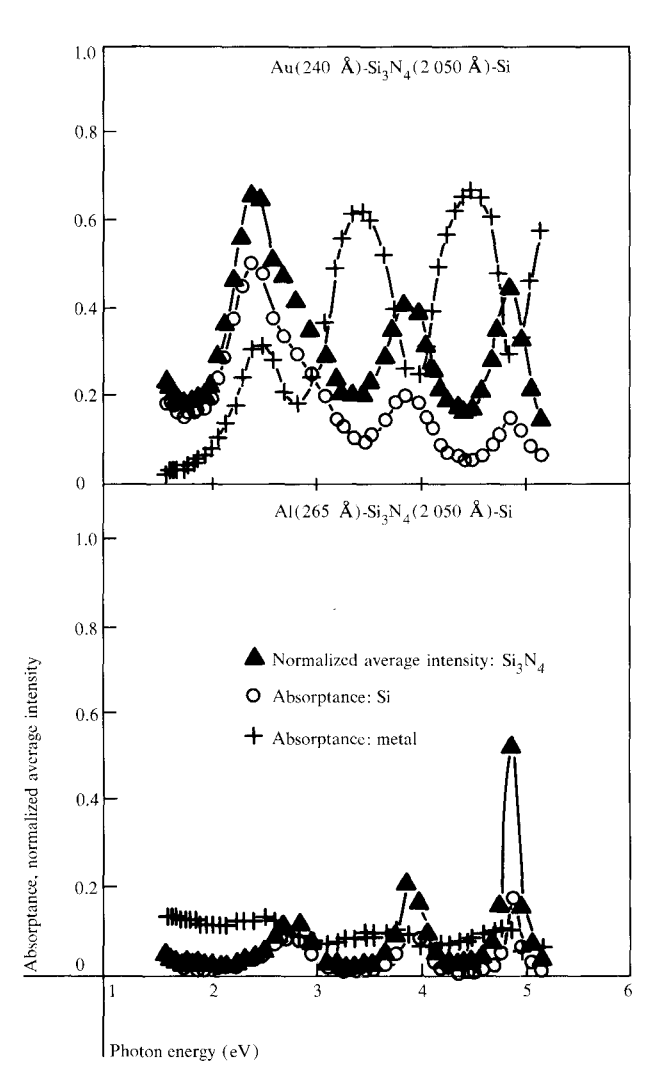


Figure 14 Theoretical calculations of the absorptance in the silicon and metal layers and the normalized average intensity in the silicon nitride bulk for light at normal incidence as a function of photon energy for Au  $(240\ \text{Å})$  –  $\text{Si}_3\text{N}_4(2050\ \text{Å})$  – Si and Al  $(265\ \text{Å})$  –  $\text{Si}_3\text{N}_4(2050\ \text{Å})$  – Si MNS structures. The normalization for the average intensity is the incident light intensity.

relative to the calculated steady state characteristics results from the data-taking sequence, that is, the low current values do not have sufficient time to build up a steady state space charge distribution. If the data are taken from high to low current values, the slope is steeper than calculated steady state because of excess space charge at low currents.

The thickness dependence of the J- $E_{\rm av}$  characteristic in the 425 to 2050 Å range is predicted rather well by the model. The thinnest (220 Å) and thickest (3100 Å) samples deviate substantially from the predicted behavior. However, this may be due to the difficulty in obtaining consistent film properties at the extremes in thickness.

#### • Photocurrents

The photocurrent data of Fig. 10 are too strongly field dependent to be explained just by Schottky barrier lowering, including field penetration into the Si for a dominant hole injection mechanism. Hole scattering in the potential well near the  $\text{Si-Si}_3\text{N}_4$  interface was therefore included in a manner similar to electron scattering for the  $\text{Si-SiO}_2$  interface [21]. It was assumed that the photocurrents of Fig. 10 for MNS structures with  $\text{Si}_3\text{N}_4$  layers 425 Å thick could be fit to the following equations of internal photoemission [25]:

$$I_{p} = \frac{BS}{\hbar\omega} \left[ \hbar\omega - q\phi \right]^{p} e^{-\left[x_{o}(E_{o})/l\right]}, \tag{8}$$

$$\phi = \phi_{b0} - (qE_0/4\pi\epsilon')^{\frac{1}{2}} - \psi_s, \tag{9}$$

$$x_0 = (q/16\pi\epsilon' E_0)^{\frac{1}{2}},\tag{10}$$

$$E_0 = E(0) + \frac{1}{\epsilon} \int_0^{x_0} q \, n_{\rm t}(x, t) \, dx, \tag{11}$$

where B is a constant which can depend on photon energy; t is time; p is an exponent related to the hole energy distribution at the  $Si-Si_3N_4$  interface (p=2 for a step distribution or p = 3 for a ramp distribution [37, 38] are used here);  $x_0$  is the position of the potential maximum of the energy barrier (zero total field point);  $E_0$  is the field (not including that due to the image force) at  $x_0$ ; and l is the hole scattering length which measures how far a photoexcited hole will move into the Si<sub>2</sub>N<sub>4</sub> from the Si-Si<sub>3</sub>N<sub>4</sub> interface before it scatters back to this interface through the image charge potential well near that interface. In Fig. 11, we have made the approximation for the range of fields of interest that  $E_0 \approx E(0)$ ; that is, the trapped space charge between  $x_0$  and the Si-Si<sub>2</sub>N<sub>4</sub> interface is much smaller than the total trapped space charge in the Si<sub>2</sub>N<sub>4</sub> layer [6, 7]. However, this approximation may be breaking down at low applied fields; that is,  $x_0$ may be far enough into the bulk of the Si<sub>2</sub>N<sub>4</sub> film that the charge between it and the Si-Si<sub>3</sub>N<sub>4</sub> interface should be included. This correction is difficult because the charge distribution must be known.

The theoretical curves in Fig. 8 (normalized energy barrier height as a function of the square root of the field near the Si-Si<sub>3</sub>N<sub>4</sub> interface) were determined from Eq. (9) with the assumption that  $E_0 \approx E(0)$ . Values for  $\psi_s$  for various fields E(0) follow a classical treatment for an 0.001  $\Omega$ -cm n-type Si semiconductor biased in depletion, where it is assumed that Fermi-Dirac statistics hold and the bulk doping of the semiconductor is uniform with the donor level represented by a delta function density of states with normal activation energy [39, 40]. Calculations for  $\psi_s$  with the donors completely ionized or with numerically zero activation energy give similar values for  $\psi_s$  over the range of electric fields of interest. The

inclusion in Eq. (9) of the potential drop in the Si,  $\psi_s$ , is valid as long as most of the photoexcited holes reaching the Si-Si<sub>3</sub>N<sub>4</sub> interface and being involved in internal photoemission are not generated near this interface. This is a reasonable assumption if one considers that hot-hole mean free paths for optical-phonon scattering in Si are approximately 40 Å [41] and light will penetrate into the Si to at least a depth of 50 Å for the wavelengths of interest [31-33], but the depletion widths in the 0.001  $\Omega$ -cm n-Si layer are only 1 to 15 Å for the range of fields at the Si-Si<sub>n</sub>N<sub>s</sub> interface studied here [39, 40].

## • Optical interference

Much of the structure (peaks and valleys) in the photoresponse data of Figs. 4 and 5 is due to optical interference in the thin film MNS structures. By using the photon energy position of these peaks, insight into the origin (electrode or bulk) of the photocarriers may be obtained [42]. For normally incident light, theoretical calculations were made of the absorptance in the Si and metal layers [43] and the average intensity in the Si<sub>2</sub>N<sub>4</sub> layer using the appropriate optical constants for Al [27-29], Au [27, 28, 30],  $Si_3N_4$  [31], and Si [31-33] for the MNS structures shown in Figs. 4 and 5. Figure 14 shows selected results for such a calculation on MNS structures with Si<sub>2</sub>N<sub>2</sub> layers 2050 Å thick for both Au and Al metal electrodes. The derivation for the absorptance (ratio of absorbed photon energy to incident energy) in the Si and metal layers, including optical interference, follows the treatment of Berning [43] and will not be repeated here. The derivation for the average intensity in the Si<sub>3</sub>N<sub>4</sub> layer is discussed in the Appendix. Average intensity is defined here as the average of the net electric field squared (associated with the light waves) at any point in the Si<sub>3</sub>N<sub>4</sub> layer multiplied by the refractive index of Si<sub>3</sub>N<sub>4</sub>; in Fig. 14, the average intensity is normalized to the incident light intensity. Several observations can be made from Fig. 14 which are in general true for calculations for any Si<sub>3</sub>N<sub>4</sub> thickness from 220 to 3100 Å:

- For Al-Si<sub>3</sub>N<sub>4</sub>-Si MNS structures, interference peaks and valleys in the absorptance (Si or metal) and normalized average intensity (Si<sub>3</sub>N<sub>4</sub> bulk) are in phase with one another.
- 2. For Au-Si<sub>3</sub>N<sub>4</sub>-Si MNS structures, interference peaks and valleys in the absorptance of the Au layer are out of phase with peaks and valleys in the absorptance of the Si layer, and also in the normalized average intensity of the Si<sub>3</sub>N<sub>4</sub> bulk for photon energies greater than 3 eV.
- Interference peaks and valleys in the absorptance of the Si layer and normalized average intensity of the Si<sub>3</sub>N<sub>4</sub> bulk are in phase for MNS structures with either Au or Al gate metallizations.

This difference in optical interference effects between MNS structures with Al and Au electrodes is believed to be due to the difference in the photon energy dependence of the index of refraction of these two metals. Comparing the theoretical optical interference patterns like those of Fig. 14 (for a Si<sub>3</sub>N<sub>4</sub> layer 2050 Å thick) with the relevant photoresponse data of Figs. 4 and 5, the following general conclusions seem valid:

- 1. For Al-Si<sub>3</sub>N<sub>4</sub>-Si MNS structures with Si<sub>3</sub>N<sub>4</sub> thicknesses from 220 to 3100 Å, peaks in the experimental photoresponse data for either voltage polarity approximately align with peaks in the absorptance of the Si or Al or with peaks in the normalized average intensity of the Si<sub>3</sub>N<sub>4</sub> bulk. No conclusive statements can be made about the origin of photocarriers for this structure.
- 2. For Au-Si<sub>3</sub>N<sub>4</sub>-Si MNS structures with Si<sub>3</sub>N<sub>4</sub> thicknesses greater than 425 Å, peaks in the experimental photoresponse data for either voltage polarity approximately align with peaks in the absorptance of the Si or with peaks in the normalized average intensity of the Si<sub>3</sub>N<sub>4</sub> bulk. For these Au gate MNS structures, the origin of the dominant photocarriers, at least at photon energies greater than 3.5 eV and silicon nitride thicknesses greater than 425 Å, is either the Si substrate or the Si<sub>3</sub>N<sub>4</sub> bulk or both for either voltage polarity.

The definition used for the photoresponse (photocurrent density divided by the photon flux transmitted through the top metal electrode) in Section 3, "Photocurrents," could have been defined in terms of the incident light intensity, absorbed light intensity in the Si or metal layer [42], or the average light intensity in the bulk of the Si<sub>2</sub>N<sub>4</sub> film. The latter two definitions are probably more accurate if the source (Si, metal, or Si<sub>2</sub>N<sub>4</sub>) of the photocarriers is known. The cube root of the photoresponse was plotted as a function of photon energy for the various definitions given here using the same experimental data for the photocurrents as in Figs. 4 and 5. Calculated values for the absorptance in the Si or metal layers or the normalized average intensity in the Si<sub>2</sub>N<sub>4</sub> bulk such as those shown in Fig. 14 were used in calculating the photoresponse. The following general observations were made from these calculations:

- Normalizing the photocurrent to the incident light intensity yielded results very similar to those in Figs. 4 and 5.
- Normalizing the photocurrent to the absorbed intensity in the Si layer or the average intensity in the Si<sub>3</sub>N<sub>4</sub> bulk never completely smoothed out the structure because of the optical interference effects present in Figs. 4 and 5, although the radical fluctuations were suppressed.

239

Normalizing the photocurrent to the absorbed intensity in the metal layer usually enhanced the structure in the cube root photoresponse-photon energy curves, especially for the Au-Si<sub>3</sub>N<sub>4</sub>-Si MNS structures.

Corrections of the photoresponse to include scattering of photoexcited carriers in the Si or metal layers by optical phonons or by other carriers were made in some cases. Scattering corrections should be most important in the Si layer for photon energies between two and three eV, where the light is penetrating deeply into the Si layer. For this case, where the scattering length for photoexcited holes is small (less than 100 Å [41]) compared to the reciprocal of the optical absorption coefficient of Si (0.1 to 1 micrometer), previously reported photoresponse data [1] on an Al-Si<sub>2</sub>N<sub>4</sub> (220 Å) -n-degenerate Si MNS structure were corrected to include scattering. This correction is performed by normalizing the photoresponse to the Si optical absorption coefficient [44]. From a least squares fit of the cube root of the corrected photoresponse as a function of the photon energy, the energy barrier height obtained for hole internal photoemission from the Si valence band to the  $Si_3N_4$  valence band was, within  $\pm 0.1$  eV, the same as reported previously [1].

The theoretical calculations of the reflectance from MNS structures for a 10° angle of incidence like that shown in Fig. 12 follow the treatment given in Born and Wolf [45] and will not be repeated here. The theoretical reflectances for the photon energy range in Fig. 12 for the transverse electric wave (TE) and transverse magnetic wave (TM) are approximately identical at a 10° angle of incidence.

In the theoretical calculations for the absorptance (Si and metal layers), the average intensity (Si<sub>3</sub>N<sub>4</sub> bulk), and the reflectance, the finite bandpass of the monochromator was not taken into account. This approximation for the Si<sub>3</sub>N<sub>4</sub> thickness range (200 to 3100 Å) is valid because the energy width associated with a 5-m $\mu$ m bandpass is 0.01 eV and 0.1 eV at wavelengths of 8 000 Å (1.55 eV) and 2400 Å (5.2 eV), respectively, which covers the wavelength range studied here. These energy widths are small in comparison with widths of the appropriate interference peaks in the absorptance, normalized average intensity, and reflectance even on the thicker Si<sub>2</sub>N<sub>4</sub> MNS structures. See Figs. 12 and 14.

#### 5. Discussion

## Dark currents

We have reported previously [2] that, in general, the dark-current average field characteristics as a function of electrode material and nitride thickness suggest that both carriers play a role in each voltage polarity. How-

ever, for data at negative Al and Au bias, the effect of the secondary carriers (in this case, electrons) is minimal except at the highest fields, where Al currents appear to be enhanced by electrons injected from the Al electrode and trapped in the insulator, thereby reducing the positive space charge and increasing the dominant hole current. We ignore this slight secondary carrier effect and provide an analytical description of the negative bias dependence on nitride thickness in terms of a hole-carrier, single-trap-level model for the insulator.

The difference between positive Al and positive Au bias data indicates that holes are injected from the metal electrode. On the other hand, our flat-band measurements and the "carrier-type" measurements of others [5] indicate electrons may be the dominant carrier in this bias, at least with Al electrodes. The analytical description of a two-carrier problem is beyond the scope of the present study; however, it is easy to visualize that greater hole injection by the Au electrode due to the lower barrier height [1] would increase a dominant electron current through a reduction of the negative space charge by recombination or hole trapping. That the negative space charge is, in fact, reduced with the Au electrode has been verified by flat-band measurements and the magnitude of the reduction accounts for the different current levels observed in Figs. 2(b) and 3(b) [8].

We have observed that contact effects are most apparent in thin nitride structures. An explanation for this observation is apparent in the calculated curves of Fig. 13, where the contact current field characteristic has been included for comparison. Even for the large trap density of this example, it is nevertheless evident that the average field characteristic of the thinnest nitride most nearly reflects the contact current-field behavior.

The question arises as to whether the average field characteristics of thick nitrides reflect a bulk nitride conduction property. There is no unique bulk currentfield relation because, in the context of our model, the local bulk current depends on both the local field and the local trapped charge density. Note that these quantities vary across the film in such a way that current is spatially constant under steady-state conditions. We find by calculation, however, that the trapped charge density near the counter electrode changes by less than a factor of two while the current ranges from  $10^{-11}$  to  $10^{-5}$  A. Also, for thicker nitride films the average field approaches the field near the counterelectrode. Thus, we conclude that the average field characteristic of thicker films approaches the field dependence of the bulk nitride current. In summary, we find that at no thickness is the conduction process purely contact-limited or bulk-limited; however, thin nitride layers approach a contact-limited characteristic and thick layers approach a bulk-limited characteristic.

#### • Photocurrents

Previously reported results on very thin (220 to 230 Å)  $Si_3N_4$  MNS structures implied that internal photoemission dominated by hole injection was occurring for either voltage polarity [1]. Experimental evidence presented here suggests that as the  $Si_3N_4$  layer is made thicker and as trapped space charge effects become more important there is a transition from a mostly contact (internal photoemission) to mostly bulk (photoconductivity) controlled conduction mechanism. This experimental evidence, shown in Figs. 4, 5, and 14; Sections 3, "Photocurrents," and 4, "Optical interference;" and Ref. [1] is the following:

- 1. The polarity dependence of the photocurrents decreases with increasing Si<sub>2</sub>N<sub>4</sub> thickness.
- The dependence on injecting contact material (Si, Al, Au, or Mg) of the low energy intercept of the cube root of the photoresponse decreases with increasing Si<sub>3</sub>N<sub>4</sub> thickness.
- 3. Interference structure in the photoresponse data aligns regardless of voltage polarity or gate metal, at least for photon energies greater than 3.5 eV and for Si<sub>3</sub>N<sub>4</sub> layers thicker than 425 Å. The energy position of this structure in the experimental data is in phase (at least for Au-Si<sub>3</sub>N<sub>4</sub>-Si MNS structures) with theoretical calculations for the average intensity in the Si<sub>3</sub>N<sub>4</sub> bulk or the absorptance in the Si.

For negative gate polarity, experimental photocurrent data on Si<sub>2</sub>N, MNS structures 425 Å thick were modeled and interpreted as dominant hole internal photoemission from the Si valence band, at 2.1 eV and conduction band, at 3.2 eV, into the Si<sub>3</sub>N<sub>4</sub> valence band. These two thresholds for hole internal photoemission are apparent to some degree in all the data presented in Figs. 4(a) and 5(a) regardless of Si<sub>3</sub>N<sub>4</sub> thickness and optical interference effects, and they are independent of gate metallization. The linear intensity dependence of the photocurrents described in Section 3, "Photocurrents," and Fig. 6, is also consistent with internal photoemission [21, 22]. The experimental field dependence of the 3.2 eV energy barrier tends to agree with simple barrierlowering theory, which includes the Schottky effect and field penetration. However, experimental data for the 2.1 eV energy barrier are smaller quantities than predicted theoretical values at high fields; this effect may be due to tunneling of photoexcited carriers.

For continuous light irradiation the cube root of the photoresponse as a function of photon energy for a 2 MV/cm average field (negative gate bias) on  $\mathrm{Si_3N_4}$  MNS structures 425 and 1000 Å thick had low energy, less than 2 eV, tails that were approximately independent of photon energy [see Figs. 4(a) and 5(a)]. This

effect may be due to photo-detrapping in the bulk of the  $Si_3N_4$  layer. Another possible explanation is photoenhancement of dark currents by removal or rearrangement with light of trapped charge near the injecting contact or by the creation of additional photoexcited carriers at the  $Si_3N_4$  interface that can tunnel into the  $Si_3N_4$ .

The photocurrent dependence on negative gate voltage for 425 Å Si<sub>3</sub>N<sub>4</sub> MNS structures is too strong to be explained only by energy barrier lowering for holes at the Si-Si<sub>2</sub>N<sub>4</sub> interface. Therefore we have included hole scattering in the Si<sub>2</sub>N<sub>4</sub> layer as a possible explanation for the observed voltage dependence. The saturation and roll-over of the photocurrent-average field data seen on Al-Si<sub>2</sub>N<sub>4</sub>(425 Å) - n-degenerate Si MNS structures (Fig. 1) and not on similar structures with p-degenerate Si substrates are probably due to an effect that reduces the number of photoexcited holes that reach the Si-Si<sub>2</sub>N<sub>4</sub> interface and participate in internal photoemission. One possible explanation is scattering of these photoexcited holes in the Si depletion region, which would be dependent on the average field and photon energy but independent of light intensity as seen experimentally.

The trapping model of Mott and Gurney [46], which Goodman has used unsuccessfully to explain photocurrents in metal-silicon dioxide-silicon (MOS) structures [47, 21], also fails here in explaining the observed photocurrent-average field data of Fig. 10. If the trapping model is applicable, then the strongly voltage dependent regions of Fig. 10 are controlled by the Schubweg, i.e., the average distance travelled by a photoinjected carrier before being trapped and immobilized in the Si<sub>2</sub>N<sub>4</sub> layer. A photocurrent arising from such a model would be mostly displacement current, and it would decrease in time as trapped holes in the Si<sub>2</sub>N<sub>4</sub> bulk establish a positive space charge layer that reduces the field at the injecting contact (Si-Si<sub>3</sub>N<sub>4</sub> interface) to zero. For photocurrents over the range of interest,  $10^{-11}$  to  $10^{-9}$  A, to be caused by a displacement current due to hole trapping would require changes in the flatband voltages of at least -6.4 volts over 10<sup>3</sup> s. However, experimental changes in the flatband voltages, controlled mostly by the dark current level for average fields ≥ 3 MV/cm, were less than -2 volts over  $10^3$  s.

For many fields of interest where  $x_0 < 10 \text{ Å}$  (Fig. 11), the validity of the macroscopic continuum model used here as opposed to a discrete charge model may be questionable. Also, the small, energy-dependent values of l (less than one Å) as obtained from data fitting, and the possibility of composition variation of the  $\mathrm{Si_3N_4}$  near the  $\mathrm{Si\text{-}Si_3N_4}$  interface, may imply that use of the Berglund-Powell scattering model used in this investigation is not completely adequate. These questions, although relevant, are beyond the scope of this study.

#### • Similarities

Dark currents and photocurrents similarly reflect contact and  $Si_3N_4$  thickness dependences, and both show a transition from a more nearly contact-controlled to a more nearly bulk-controlled conduction mechanism with increasing  $Si_3N_4$  thickness. More specifically, the similarities which are apparent from Figs. 2-5 and Refs. 1 and 2 are the following:

- Both currents reflect the contacts and the importance of hole injection in thin Si<sub>3</sub>N<sub>4</sub> MNS structures.
- 2. Both currents decrease in a similar manner as the Si<sub>2</sub>N<sub>4</sub> layer thickness is increased.
- With both currents, voltage polarity differences decrease, especially for Al gate MNS structures, as the Si<sub>3</sub>N<sub>4</sub> thickness is increased.

#### 6. Conclusions

The importance of hole injection, conduction, and trapping has been demonstrated in MNS structures. A transition from contact- to bulk-controlled conduction has been shown with increasing thickness of a silicon nitride layer. For negative gate voltage bias, dominant hole conduction mechanisms and trapped space charge effects have been modeled for both dark current and photocurrent data. For positive gate voltage bias, where both electrons and holes may be important in the conduction process, qualitative explanations of the experimental data have been given.

As has been demonstrated here and in other recent publications by the authors [1, 2, 8], silicon nitride is a very complicated insulator from the viewpoint of conduction and trapping as compared to the thermal silicon dioxide commonly used as the insulating layer in silicon technology. By contrast, silicon dioxide has very low electronic conduction and minimal trapping. The charge transport mechanism in silicon nitride is essentially a two-carrier problem that is further complicated by the trapping of both holes and electrons in the bulk of the film. These trapped charges in turn cause strong internal electric fields to develop which affect both the bulk silicon nitride conduction and charge carrier injection into the insulator from the contacts. Clearly, any further experimental or theoretical investigations should be performed with these points in mind.

# Acknowledgments

The authors acknowledge the critical reading of this manuscript by A. B. Fowler and helpful discussions with A. B. Fowler, E. A. Irene, C. M. Osburn, N. Klein, B. H. Yun, P. Solomon, S. Zirinsky, and F. Stern. The experimental assistance of H. Ripke, M. J. Smyth, and J. A. Kucza, and the assistance of E. A. Irene, who provided the samples; of E. D. Alley and J. Dempsey, who

performed the metallizations; of E. A. Spiller, who provided the computer programs used in calculating the absorptance in the silicon and metal layers and the reflectance of the entire MNS structure; and of F. Stern, who provided the computer program used in calculating the surface potential of the silicon, is also gratefully acknowledged.

#### Appendix: Average light intensity

Bulk insulator photoconductivity may arise from photoexcitation of trapped electrons or holes into their respective bands or, for sufficiently high photon energies, by electron-hole creation across the insulator optical bandgap. Both of these processes are proportional to the square of the electric field resulting from the interference of incident and reflected light waves. This interference can cause dramatic spatial fluctuations in the electric field magnitude associated with the incident light across the insulator. At the antinodes (maxima) of the electric field, for photon energies less than the band gap, the conductivity may be enhanced by photo-detrapping, causing a reduction in trapped space charge in that region. Trapped space charge will accumulate at the nodes (minima) of the electric field, giving rise to locally enhanced dark conductivity by thermal detrapping processes.

A theoretical analysis taking account of these spatial variations in light intensity (proportional to the electric field squared) and trapped charges is too complex to be treated here. Instead, we calculate the average light intensity in the insulator and look for correlations of fluctuations in the average amplitude as a function of photon energy with measured photocurrents. To facilitate comparison to the absorptance in the metal and silicon, we multiply the average field squared by the appropriate constants to give the units of energy flux and normalize to the incident photon flux.

The capacitor structure of Fig. 1 causes multilayer interference of light incident normally on the metal. For notational convenience the layers are numbered sequentially, beginning with zero for air. The electromagnetic fields propagating in the z direction are represented by

$$E_{nx} = E_{nx}^{+} e^{i\hat{k}_{n}z_{n}} + E_{nx}^{-} e^{-i\hat{k}_{n}z_{n}},$$

$$H_{ny} = \frac{c \hat{k}_{n}}{\mu \omega} \cdot \left[ E_{nx}^{+} e^{i\hat{k}_{n}z_{n}} - E_{nx}^{-} e^{-i\hat{k}_{n}z_{n}} \right],$$
(A1)

where the numerical subscript identifies the layer and  $\hat{k}_n = 2\pi (n_n + ik_n)/\lambda$  is the complex wave number of the *n*th layer with  $n_n$  and  $k_n$  the refractive index and extinction coefficient, respectively.  $E_{nx}^+$  and  $E_{nx}^-$  are the amplitudes of the forward and reverse propagating waves. We assume only a forward propagating wave in the silicon (layer 3) and match boundary conditions at the inter-

faces in the customary way (see, e.g., Heavens [48]) to obtain the electric field amplitudes in the insulator

$$E_{2x} = E_{2x}^{+} \left[ e^{i\hat{k}_2 z_2} + \hat{r}_3 e^{2i\hat{k}_2(d_2 - z_2)} \right],$$

where  $\hat{r}_n = \frac{(\hat{k}_{n-1} - \hat{k}_n)}{(\hat{k}_{n-1} + \hat{k}_n)}$  is the Fresnel reflection coefficient.

The absolute magnitude of the field squared is then

$$\begin{split} \left(E_{2x}\right)^2 &= \left|E_{2x}^+\right|^2 \left\{e^{-4\pi k_2 d_2/\lambda}\right\} \\ &\quad \times \left\{e^{4\pi k_2 (d_2 - z_2)/\lambda} + \left|r_3\right|^2 e^{-4\pi k_2 (d_2 - z_2)/\lambda} \right. \\ &\quad + 2r_3^R \cos\left[4\pi n_2 (d_2 - z_2)/\lambda\right] \\ &\quad - 2r_3^I \sin\left[4\pi n_2 (d_2 - z_2)/\lambda\right], \end{split} \tag{A2}$$

where

$$|r_3|^2 = \frac{(n_2 - n_3)^2 + (k_2 - k_3)^2}{(n_2 + n_3)^2 + (k_2 + k_3)^2},$$

$$r_3^R = \frac{n_2^2 + k_2^2 - n_3^2 - k_3^2}{(n_2 + n_3)^2 + (k_2 + k_3)^2},$$
(A3)

and

$$r_3^I = \frac{2(n_3 k_2 - n_2 k_3)}{(n_2 + n_3)^2 + (k_2 + k_3)^2}$$

are the absolute magnitude squared, the real, and the imaginary part, respectively, of  $r_3$ . The thickness of the insulator is  $d_2$ , and  $z_2$  is the distance into the insulator from the metal interface.

The average intensity is obtained by a straightforward integration of Eq. (A2) over the insulator thickness

$$\begin{aligned} |\overline{E_{2x}}|^2 &= |E_{2x}^+|^2 e^{-\beta_2} \left\{ (e^{\beta_2} - 1) / \beta_2 \right. \\ &- (e^{-\beta_2} - 1) |r_3|^2 / \beta_2 \\ &+ 2 r_3^R \sin(\alpha_2) / \alpha_2 \\ &- 2 r_2^I (1 - \cos\alpha_2) / \alpha_2 \right\}, \end{aligned}$$
(A4)

where  $\beta_n = 4\pi k_n d_n/\lambda$  and  $\alpha_n = 4\pi n_n d_n/\lambda$ . The amplitude  $E_{2x}^+$  is related to the amplitude of the incident wave  $E_{0x}^+$  by

$$|E_{2x}^+|^2 = \frac{|t_1|^2 |t_2|^2 e^{-\beta_1} |E_{0x}^+|^2}{(\text{DENOM}^R)^2 + (\text{DENOM}^I)^2},$$
 (A5)

where  $t_n=2~\hat{k}_{n-1}/~(\hat{k}_{n-1}+\hat{k}_n)$  is the Fresnel transmission coefficient, so that

$$t_n^2 = \frac{4[n_{n-1}^2 + k_{n-1}^2]}{(n_{n-1} + n_n)^2 + (k_{n-1} + k_n)^2}.$$

Also

$$\begin{split} \text{DENOM}^{R} &= 1 + e^{-\beta_{1}} \{ r_{12}^{R} \cos \alpha_{1} - r_{12}^{I} \sin \alpha_{1} \} \\ &+ e^{-\beta_{2}} \{ r_{23}^{R} \cos \alpha_{2} - r_{23}^{I} \sin \alpha_{2} \} \\ &+ e^{-(\beta_{1} + \beta_{2})} \{ r_{13}^{R} \cos (\alpha_{1} + \alpha_{2}) \\ &- r_{13}^{I} \sin (\alpha_{1} + \alpha_{2}) \} \end{split}$$

and

$$\begin{split} \text{DENOM}^I &= e^{-\beta_1} \{ r_{12}^I \cos \alpha_1 + r_{12}^R \sin \alpha_1 \} \\ &+ e^{-\beta_2} \{ r_{23}^I \cos \alpha_2 + r_{23}^R \sin \alpha_2 \} \\ &+ e^{-(\beta_1 + \beta_2)} \{ r_{13}^I \cos (\alpha_1 + \alpha_2) \\ &+ r_{13}^R \sin (\alpha_1 + \alpha_2) \}, \end{split}$$

where  $r_{nm}^R$  and  $r_{nm}^I$  are the real and imaginary parts of the complex product  $\hat{r}_n\hat{r}_m$  of Fresnel reflection coefficients and are given in terms of the definitions in Eq. (A3):

$$r_{nm}^{R} = r_{n}^{R} r_{m}^{R} - r_{n}^{I} r_{m}^{I}$$
, and 
$$r_{nm}^{I} = r_{n}^{R} r_{m}^{I} + r_{n}^{I} r_{m}^{R}$$
.

Thus, Eqs. (A4) and (A5) relate  $|\overline{E}_{2x}|^2$  to  $|E_{0x}^+|^2$ . For comparison to the absorptance in the metal and silicon layers, we also normalize the average intensity to incident flux and plot the quantity  $n_2 |\overline{E}_{2x}|^2 / n_0 |E_{0x}^+|^2$ . Even the average intensity shows dramatic fluctuations as a function of photon energy, as is shown in Fig. 14.

#### References and notes

- D. J. DiMaria and P. C. Arnett, Appl. Phys. Lett. 26, 711 (1975).
- P. C. Arnett and D. J. DiMaria, Appl. Phys. Lett. 27, 34 (1975).
- 3. B. H. Yun, Appl. Phys. Lett. 27, 256 (1975).
- Z. A. Weinberg and R. A. Pollack, Appl. Phys. Lett. 27, 254 (1975).
- A. S. Ginovker, V. A. Gritsenko, and S. P. Sinitsa, Phys. Status Solidi A 26, 489 (1974).
- 6. B. H. Yun, Appl. Phys. Lett. 25, 340 (1974).
- P. C. Arnett and B. H. Yun, Appl. Phys. Lett. 26, 94 (1975).
- P. C. Arnett and D. J. DiMaria, J. Appl. Phys. 47, 2092 (1976).
- G. A. Brown, W. C. Robinette, and H. G. Carlson, J. Electrochem. Soc. 115, 948 (1968).
- K. Tanabashi and K. Kobayashi, Jap. J. Appl. Phys. 12, 641 (1973)
- 11. E. A. Taft, J. Electrochem. Soc. 118, 1341 (1971).
- 12. S. M. Sze, J. Appl. Phys. 38, 2951 (1967).
- J. R. Yeargan and H. L. Taylor, J. Electrochem. Soc. 115, 273 (1968).
- V. Y. Doo, D. R. Nichols, and G. A. Silvey, J. Electrochem. Soc. 113, 1279 (1966).
- T. L. Chu, C. H. Lee, and G. A. Gruber, J. Electrochem. Soc. 114, 171 (1967).
- H. Maes and R. Van Overstraeten, Appl. Phys. Lett. 27, 282 (1975).
- A. S. Grove, Physics and Technology of Semiconductor Devices, John Wiley & Sons, Inc., New York, 1967, Chs. 9 and 11
- S. M. Sze, Physics of Semiconductor Devices, John Wiley & Sons, Inc., New York, 1969, Ch. 9.
- 19. L. Sullivan and H. C. Card, J. Phys. D 7, 1531 (1974).

- C. M. Osburn, IBM Thomas J. Watson Research Center, has also observed the polarity difference in dark-current data for Al gate Si<sub>4</sub>N<sub>4</sub> MNS structures.
- 21. C. N. Berglund and R. J. Powell, J. Appl. Phys. 42, 573 (1971).
- D. J. DiMaria, F. J. Feigl, and S. R. Butler, *Phys. Rev. B* 11, 5023 (1975).
- M. A. Lampert and P. Mark, Current Injection in Solids, Academic Press Inc., New York, 1970.
- 24. D. J. DiMaria, J. Appl. Phys. 45, 5454 (1974).
- R. J. Powell and C. N. Berglund, J. Appl. Phys. 42, 4390 (1971).
- 26. D. J. DiMaria and F. J. Feigl, Phys. Rev. B 9, 1874 (1974).
- L. G. Schulz and F. R. Tangherlini, J. Opt. Soc. Am. 44, 362 (1954).
- 28. L. G. Schulz, J. Opt. Soc. Am. 44, 357 (1954).
- G. Hass and J. E. Waylonis, J. Opt. Soc. Am. 51, 719 (1961).
- 30. D. Beaglehole, Proc. Phys. Soc. (Lond.) 85, 1007 (1965).
- 31. H. R. Philipp and E. A. Taft, Phys. Rev. 120, 37 (1960).
- H. R. Philipp and H. Ehrenreich, Phys. Rev. 129, 1550 (1963).
- 33. W. C. Dash and R. Newman, Phys. Rev. 99, 1151 (1955).
- 34. H. R. Philipp, J. Electrochem. Soc. 120, 295 (1973).
- 35. P. C. Arnett, J. Appl. Phys. 46, 5236 (1975).
- M. A. Lampert and P. Mark, Current Injection in Solids, Academic Press Inc., New York, 1970, p. 147.
- 37. R. H. Fowler, Phys. Rev. 38, 45 (1931).

- 38. R. J. Powell, J. Appl. Phys. 41, 2424 (1970).
- The surface potential was calculated using a program written by F. Stern, IBM Thomas J. Watson Research Center.
- A. Many, Y. Goldstein, and N. B. Grover, Semiconductor Surfaces, North-Holland, Amsterdam, 1965, Ch. IV.
- C. R. Crowell and S. M. Sze, *Physics of Thin Films*, edited by G. Hass and R. E. Thun, Academic Press Inc., New York, 1967, vol. 4, pp. 325-371.
- 42. R. J. Powell, J. Appl. Phys. 40, 5093 (1969).
- P. H. Berning, *Physics of Thin Films*, edited by G. Hass, Academic Press Inc., New York, 1963, vol. 1, pp. 69-121.
- T. H. DiStefano and J. E. Lewis, J. Vac. Sci. Technol. 11, 1020 (1974).
- 45. M. Born and E. Wolf, *Principles of Optics*, Pergamon Press Inc., New York, 1964, 3rd ed., Ch. 1.
- N. F. Mott and R. W. Gurney, Electronic Processes in Ionic Crystals, Oxford, Clarendon Press, London, 1948, 2nd ed., Ch. IV.
- 47. A. M. Goodman, Phys. Rev. 144, 588 (1966).
- 48. O. S. Heavens, Optical Properties of Thin Solid Films, Academic Press Inc., New York, 1955, Ch. 4.

Received May 24, 1976; revised October 14, 1976

The authors are located at the IBM Thomas J. Watson Research Center, Yorktown Heights, New York 10598.